

MIT Open Access Articles

Effective Size and Zeta Potential of Nanorods by Ferguson Analysis

The MIT Faculty has made this article openly available. **Please share** how this access benefits you. Your story matters.

Citation: Park, Sunho, Niraj Sinha, and Kimberly Hamad-Schifferli. "Effective Size and Zeta Potential of Nanorods by Ferguson Analysis." *Langmuir* 26.16 (2010) : 13071-13075.

As Published: <http://dx.doi.org/10.1021/la1024108>

Publisher: American Chemical Society

Persistent URL: <http://hdl.handle.net/1721.1/65164>

Version: Author's final manuscript: final author's manuscript post peer review, without publisher's formatting or copy editing

Terms of Use: Article is made available in accordance with the publisher's policy and may be subject to US copyright law. Please refer to the publisher's site for terms of use.



Effective Size and Zeta-Potential of Nanorods by Ferguson Analysis

Sunho Park¹, Niraj Sinha¹ and Kimberly Hamad-Schiffertli^{1,2}

¹Department of Mechanical Engineering and ²Department of Biological Engineering

Massachusetts Institute of Technology, 77 Massachusetts Ave, Cambridge, MA 02139

AUTHOR EMAIL ADDRESS schiffertli@mit.edu

RECEIVED DATE

CORRESPONDING AUTHOR FOOTNOTE schiffertli@mit.edu

ABSTRACT Effective hydrodynamic size and free mobility of particles of varying aspect ratio were evaluated by Ferguson analysis of gel electrophoresis. Ligand layer thickness was estimated from the difference between the effective size and the size of metal core from TEM imaging. Zeta-potential of the particles was calculated from the Ferguson analysis result by applying conventional electrophoresis theories for spheres and cylinders. Results show that Henry's solution for spherical particles can be used to obtain the zeta-potential of cylindrical particles without requiring the use of TEM for size analysis.

KEYWORDS Ferguson analysis, gel electrophoresis, gold nanoparticle, gold nanorod, free mobility, zeta-potential, Henry's solution

Introduction

Gold nanoparticles (AuNPs) have been attractive for a broad range of biological applications such as delivery, diagnosis and control.¹⁻⁴ Because their optical properties can vary dramatically with particle shape,⁵ one can tune NP absorption throughout the tissue window in the infrared simply by changing synthesis conditions.⁶⁻¹⁰ Consequently, AuNPs have been made in a variety of shapes such as rods, shells, moons, and stars.¹¹⁻¹⁶ For all of these particles, their interface to biomolecules and cells influences their biological behavior and consequences. In particular, previous work has determined that NP hydrodynamic size (D_H) and zeta potential (ζ) are key parameters for quantitatively understanding NP cell uptake, stability in biological fluids, propensity for aggregation, and protein adsorption. For example, NPs have been developed for gene delivery. It has been found that particle size, shape and ζ all influence their transport, cellular uptake, and ability to deliver payloads, which all impact overall therapeutic efficacy.¹⁷⁻²¹ Furthermore, ζ is a measure of the tendency of particle aggregation and non-specific adsorption to proteins, which can cause undesirable biological side effects.²² Thus, measurement of these parameters is essential for quantifying and understanding not only the intended but also unintended biological responses of NPs.

Typically, commercial zeta-potentiometers are used to measure free mobility (M_0) and D_H of NPs, which then convert the information into ζ by using simple theoretical formulas approximating the NP as a sphere. Those devices are based on a dynamic light scattering (DLS) method, which is well-established for relatively large and spherical biopolymers or colloids. However, they often fail to produce consistent and accurate estimates for ζ when the particle shape is not spherically symmetric because they assume the correlation functions are generated from spheres. In addition, particle surface chemistry more complicated than a completely uniform monolayer of a small molecule, such as a polymer in either single layer or multilayer form, disturbs the particle hydrodynamics and causes deviations from that of hard sphere. Subsequently, measurement of D_H for these types of particles is inaccurate and ζ is not well-determined. For cylinders, the simplest non-spherical shape, zeta-potentiometers have been used successfully for large ($> 1 \mu\text{m}$) cylinders with relatively smooth

surfaces.²³⁻²⁴ However, the gold nanorods (AuNRs) that are broadly used in biological applications are much smaller, in the 10 – 100 nm size regime, and are always modified with chemical surface ligands, biomolecules, or polymer multilayers. Consequently, the particles have a non-uniform charge distribution in addition to an irregular shape, properties which would be overlooked by a standard zeta-potentiometer measurement. Despite the biological importance of ζ and D_H , zeta-potentiometers fail to produce consistent and accurate estimates for the AuNPs that are most biologically relevant.

Previously, we determined that Ferguson analysis of gel electrophoresis was an attractive alternative to measure effective hydrodynamic size (D_{eff}), M_0 , and ζ of surface-modified spherical AuNPs.²⁵⁻²⁶ This study determined that Ferguson analysis can be much more accurate than zeta-potentiometers especially for the AuNPs that biologically applicable. Because there are several theories that have been written for non-spherical shapes, Ferguson analysis is highly suitable for extension to measure the ζ of AuNRs.

Here we extend the method to mercaptohexadecanoic acid (MHDA) coated AuNRs of different aspect ratios (ARs) in the size range of <100 nm. Gel electrophoretic mobility of AuNPs and AuNRs of two different ARs was experimentally measured and converted into ζ using conventional theories of electrophoresis. Results show that Ferguson analysis is a reliable approach for evaluating ζ of AuNRs with chemical surface modification.

Materials and Methods

Synthesis of spherical AuNPs standards with sodium citrate

AuNPs were synthesized by reduction of gold (III) chloride trihydrate ($\text{HAuCl}_4 \cdot 3\text{H}_2\text{O}$, Sigma Aldrich) in boiling water by addition of sodium citrate. Varying the sodium citrate varied the resulting AuNP size.²⁷ Average diameters of the AuNPs were 8.5 ± 1.3 , 18.5 ± 2.9 , 24.4 ± 4.2 , and 45.0 ± 3.9 nm, obtained by analysis of TEM images (JEOL 2011, Supporting information) with ImageJ software.²⁸ AuNPs were functionalized with the negatively charged ligand BPS (bis(p-sulfonatophenyl)

phenylphosphine, Strem Chemicals) and suspended in 0.5× TBE (45mM tris, 45mM boric acid, and 1mM EDTA).

Synthesis of sphere, nanorod and short-nanorod with ascorbic acid

Concentrations of reactants in each solution are listed in Table 1. $\text{HAuCl}_4 \cdot 3\text{H}_2\text{O}$ and silver nitrate (AgNO_3) were added to CTAB and sodium chloride (NaCl) solution and gently mixed by inverting the container. L-ascorbic acid (AA) was added to the solution and mixed by inversion, which made the solution transparent, and then sodium borohydride (NaBH_4) was added and mixed by inversion. The solutions were placed at room temperature for at least 12 hrs, and the color of the solution turned dark. The role of each chemical and influence of its concentration change are found in literature.¹²⁻¹³ Following a round-trip phase transfer ligand exchange method for replacing CTAB with MHDA (mercaptohexadecanoic acid) described in another work²⁹ was used to modify the AuNRs with MHDA. AuNRs modified with MHDA were finally in 0.5× TBE. UV-Visible absorption spectrum of each AuNR was recorded for quality maintenance, and TEM images (Figure 1, JEOL 2011) were analyzed with ImageJ for dimensional data.²⁸ AR was calculated by length / width.

Gel electrophoresis

Gel electrophoresis of the AuNPs and AuNRs were performed with varying agarose percentages, T ($T = 0.5 - 2.0\%$). 0.1, 0.5 and 2.0× TBE were used as gel casting and running buffer. Gel running time ($\sim 90 - 120$ min) and electric field strength (3.7 – 4.0 V/cm) were recorded. Band migration distances were measured by digital image capture, and the position of the band was determined by line scans down the center of the lane in the image and converted to an absolute mobility ($M = \text{velocity} / \text{electric field strength}$, [$\text{cm}^2/\text{V}\cdot\text{s}$]).

Results and Discussion

AuNR AR can be controlled. Synthesis could systematically tune the AR of the AuNRs. The presence of Ag^+ greatly affected the shape and the AR of the synthesized AuNRs. It is known that Ag^+ enhances the stability of particles so that they can maintain their rod-like shape, and without it spheres

are formed.¹² Figure 1a shows a TEM image of particles synthesized without AgNO₃, which results in a majority of spheres of diameter 24.1nm, although a few long nanorods still exist. By adding AgNO₃ and changing the amount of the reducing agent ascorbic acid, AuNRs of dimensions 30.2 × 8.8 nm (nanorods, AR ~ 3.4) or 27.5 × 15.4 nm (short nanorods, AR~ 1.8) were synthesized (Figure 1b and 1c). UV-Vis spectra shows that the surface plasmon resonance (SPR) of the spheres, NRs, and short NRs are at 528, 760 and 665 nm, respectively (Figure 1d), also supporting size and shape tunability.

Analysis of mobility for D_{eff} The mobilities, M , of the NPs and NRs were measured by agarose gel electrophoresis. Figure 2a shows one of the agarose gels with a gel percentage T of 1.0 %. Sodium citrate-reduced and BPS-coated spherical AuNPs are in lanes 1 – 4 ($D = 8.5, 18.5, 24.4$ and 45.0 nm), and ascorbic acid-reduced and MHDA-coated sphere, NRs (AR 3.4) and short NRs (AR 1.8) are in lanes 5, 6, and 7, respectively. Both BPS and MHDA are negatively charged ligands, thus all of the NPs migrate toward the positive electrode. The measured M of the particle decreases with increasing T , due to increased collisions and binding to the gel fibers. The logarithm of the mobility ($Log_{10}M$) can be linearly regressed with a Ferguson model:^{25, 30}

$$Log_{10}M = Log_{10}M_0 - K_R \cdot T \quad (1)$$

where the slope is K_R , the retardation coefficient. M can be extrapolated to $T = 0$ % to obtain an estimation of the free mobility, M_0 . Figure 2b shows a Ferguson plot of the AuNP size standards in 0.5× TBE (see Supporting Information for 0.1 and 2.0× TBE), and Figure 2c the Ferguson plots for the spheres, NRs, and short NRs. Ferguson analysis suggests an equation for K_R :

$$\sqrt{K_R} = a \cdot R + b \quad (2)$$

where R is the radius of spherical particle, and a and b are constants. The square root of the slope of Ferguson plot ($(K_R)^{1/2}$) is a function of the NP size only (Figure 2d), and does not depend on particle surface charge.²⁵ Therefore, the sodium citrate reduced spherical AuNPs of known diameters (Lanes 1 – 4, Figure 2a) can be used as sizing standards in Eq. 2.

D_{eff} of the NRs and spherical particles was obtained from the slope of the Ferguson plots using Eqs. 1 and 2. D_{eff} are shown in Figure 3a as a function of the buffer concentration (light gray, gray and dark gray column for 0.1, 0.5 and 2.0× TBE, respectively). D_{eff} of the spherical NPs from Ferguson analysis is larger than the diameter estimated by TEM (black column) due to the fact that the TEM only images the Au particles, and not the ligand. This difference is $\sim 4.3 - 4.9$ nm, which represents approximately twice the thickness of MHDA layer. This difference can be added to the TEM-measured length and diameter of NR and short-NR to determine the actual hydrodynamic length and width. Note that the BPS layer thickness was not added to the TEM size of the standard AuNPs; past molecular dynamics simulations³¹ revealed that the BPS thickness on AuNP surfaces is in the sub-nanometer range and thus relatively small. The obtained values for D_{eff} of the NRs or short NRs is somewhere in between its length and diameter as measured by TEM (white and black, Figure 3a). D_{eff} of short NRs is 20 – 22nm, close to that of the long NR, even though their surface area is almost 50% larger and the volume is twice as much (Figure 3d). Therefore, the D_{eff} of a cylindrical particle is dependent more on the particle's actual dimensions rather than surface area or volume. The fact that the obtained D_{eff} values are highly similar could be due to the fact that the average of the long and short dimensions of the NRs happens to be close in value (21.5nm for the short AR NRs and 19.5nm for the long ARs). The thickness of polymer layer on non-spherical particles can be achieved also by matching the surface area of the particle to an equivalent spherical particle,³²⁻³³ however, the method suggested in this paper is more direct.

Analysis of data for zeta-potential. ζ of the AuNPs and AuNRs was calculated from M using conventional theories. M_0 was obtained from the experimental data by extrapolating the Ferguson plot to $T = 0$ %. Henry's solution relates M_0 to ζ for spherical particles by:³⁴

$$M_0 = \frac{\epsilon \zeta}{\eta} \cdot f(\kappa R) \quad (3)$$

$$f(\kappa R) \approx \frac{2}{3} \left(1 + \frac{1}{2} \left(1 + \frac{2.5}{\kappa R} \right)^{-1} \right), \quad \frac{2}{3} < f(\kappa R) < 1 \quad (4)$$

where $1/\kappa$ is Debye length (Supporting Information), $R = D_{eff}/2$, and ε and η are the permittivity and the viscosity of the media, respectively. Ohshima's corrections to Henry's solution take into account charge relaxation around the particles, which can reduce particle M (Supporting Information for $f_3(\kappa R)$ and $f_4(\kappa R)$):³⁵

$$M_0 = \frac{\varepsilon\zeta}{\eta} \cdot \left[f(\kappa R) - \frac{2}{3} \left(\frac{ze\zeta}{k_B T_A} \right)^2 \left\{ f_3(\kappa R) + \left(\frac{m_+ + m_-}{2} \right) f_4(\kappa R) \right\} \right] \quad (5)$$

For cylindrical particles, M can differ depending on how the particle is aligned with the electric field. $M_{||}$ is defined as the mobility when the long axis of the particle is aligned with electric field, and M_{\perp} for the short axis. When particles are randomly oriented during electrophoresis and no end or relaxation effects are considered, M_0 is a weighted sum of the two different mobility values:³⁶

$$M_0 = \frac{1}{3} M_{||} + \frac{2}{3} M_{\perp} \quad (6)$$

Henry's other solution for an infinitely long cylinder of radius R is:³⁷

$$M_{||} = \frac{\varepsilon\zeta}{\eta} \quad (7)$$

$$M_{\perp} = \frac{\varepsilon\zeta}{\eta} \cdot f_{cyl}(\kappa R) \quad (8)$$

Harris suggested the upper and lower bounds of $M_{||}$ and M_{\perp} when $1/\kappa \gg R$:³⁸

$$\frac{1}{2} \frac{\varepsilon\zeta}{\eta} \leq M_{||, \perp} \leq \frac{\varepsilon\zeta}{\eta} \quad (9)$$

The lower bound of $M_{||}$ is applicable only when Debye length is very large (i.e. very weak ionic strength of the media), which is not the case for general physiological conditions. Ohshima derived an exact solution for $f_{cyl}(\kappa R)$ for all range of $1/\kappa$ and approximated it as:³⁷

$$f_{cyl}(\kappa R) \approx \frac{1}{2} \left[1 + \left(1 + \frac{2.55}{[\kappa R \{1 + \exp(-\kappa R)\}]} \right)^{-2} \right], \quad \frac{1}{2} < f_{cyl}(\kappa R) < 1 \quad (10)$$

Therefore, M_0 can be expressed as:

$$M_0 = \frac{\varepsilon\zeta}{\eta} \cdot \frac{1}{3} [1 + 2f_{cyl}(\kappa R)] = \frac{\varepsilon\zeta}{\eta} \cdot g(\kappa R), \quad \frac{2}{3} < g(\kappa R) < 1 \quad (11)$$

combining Eqs. 6 through 8. Both $f(\kappa R)$ (Eq. 4) and $g(\kappa R)$ will have similar values (2/3 or 1) when κR approaches 0 or ∞ , respectively. However, $f(\kappa R)$ and $g(\kappa R)$ differ for intermediate values of κR is used with either D_{eff} or the actual size adjusted with the polymer layer thickness.

First, ζ (Figure 3c. light gray, gray and dark gray column for 0.1, 0.5 and 2.0× TBE, respectively) was obtained from D_{eff} (Figure 3a) and M_0 (Figure 3b) using Henry's solution for spherical particles (Eqs. 3 and 4). The different TBE concentrations were chosen to demonstrate the environment of different ionic strengths. $1/\kappa$ of 0.1, 0.5 and 2.0× TBE (see Supporting Information) is 9.3, 4.1 and 2.0 nm, respectively. For the spheres, $\zeta = -43$ mV at 0.1× TBE and decreased with increasing TBE concentration due to increased ionic charge binding to the particle surface. Using the spherical assumption for the AuNRs, the NRs and short NRs had a similar value of $\zeta \sim -43$ mV at 0.1× TBE, but the ζ did not change much with increasing TBE concentration. Ohshima's correction to Henry's solution for spherical particles (Figure 3c, cross-hatched columns) typically increased ζ at all TBE concentrations by $\sim 10\%$ since a higher ζ is required to retain the same M_0 as charge relaxation around the particles causes retardation. Using the D_{eff} of NRs and short NRs (Figure 3a) and the TBE condition, κR ranges from 1.1 to 5.0 so that $f(\kappa R)$ in Eq. 4 varies from 0.77 to 0.89, an intermediate range.

Theories for cylindrical particles (Eq. 11) were applied using the actual dimensions of the AuNRs (i.e. TEM size + MHDA layer thickness) to calculate values for ζ . Obtained values of ζ (white columns, Figure 3c) for NRs and short NRs were higher than the results from the spherical approximation by $\sim 10\%$. κR using the actual AuNR radius ranges from 0.7 to 5.0, therefore $g(\kappa R)$ in Eq. 11 varies from 0.7 to 0.81. Henry's solutions for spherical particles and cylinders show approximately a 10% difference due to the difference in calculated $f(\kappa R)$ from D_{eff} and $g(\kappa R)$ from the actual size. Henry's solution for spherical particles with corrections for charge retardation (cross hatched columns) yields almost the same value as the result from the solution for cylinders. Therefore, D_{eff} from Ferguson plots seem to be the size of an equivalent sphere that retains the same ζ and M_0 of a given cylinder. When the MHDA layer thickness was ignored and only TEM sizes were put into the equations, the result of ζ differed

only by $\sim 2\%$ (results not shown). For example, when short NRs are in $0.5\times$ TBE, $\zeta = -45\text{mV}$ vs. -46mV with or without consideration of MHDA layer. ζ of AuNR found in literature is $\zeta < \pm 100\text{mV}$,^{21,23-24,39} and the ζ value here is also within this range.

Conclusions

Ferguson analysis has been shown to be feasible for determining the D_{eff} of non-spherical particles by direct interpolation from a sizing standard. The method can also quantify M_o and ζ with the aid of conventional theories of electrophoresis. For cylindrical particles, assumption of a spherical shape is reasonable for the conditions in this paper in that it gives a similar result compared with that from the cylindrical particle assumption. Because analysis for ζ with cylindrical particles requires TEM imaging to obtain both the size and width, the spherical particle assumption corrected for charge relaxation is much more convenient.

The theories for cylindrical particles used have some limitations, as they assume an infinitely long cylinder, and no charge relaxation corrections to them exist. Presumably, as the length of a cylindrical NR becomes very long, it will not be able to be randomly oriented in the agarose gel structure because of the limited gel pore size. This would require adjustments to Eq. 6.⁴⁰⁻⁴¹ Thus, testing the limits of these theories with very long cylinders would provide insight on how to improve their accuracy. Because surface modification chemistries for NRs and NPs are numerous and diverse, future work will probe the effect of surface chemistry and how it affects gel mobility and the subsequent analysis.

ACKNOWLEDGMENT We thank Center for Materials Science and Engineering at M.I.T. for use of their TEM facility. This work was supported by the NSF (DMR 0906838).

SUPPORTING INFORMATION PARAGRAPH Supporting Information includes TEM images and sizing histograms of gold NPs, Ferguson plots, and details of electrophoresis-related theories and calculations. This material is available free of charge via the Internet at <http://pubs.acs.org>



Figure 1. TEM images and sizing histograms of ascorbic acid-reduced (a) sphere, (b) NR and (c) short-NR were synthesized in CTAB and ligand-exchanged to MHDA. Size bar is equivalent to 100 nm. See Table 1 for further details of synthesis. TEM images were taken after ligand exchange with MHDA since the exchange process sometimes results in a change particle shape. (d) Absorption spectra of spheres, NRs and short-NRs. Data were normalized to the peak value of each sample. SPR peaks were at 528, 760 and 665 nm, respectively.



Figure 2. (a) One of the gels used for electrophoresis and analysis with 1.0% agarose gel in 0.5× TBE. Lane 1 – 4: 8.5, 18.5, 24.4 and 45.0 nm AuNP (sodium citrate method), respectively. Lane 5 – 7: spheres, NRs and short-NRs with MHDA ligand, respectively. Electrophoresis was repeated for 0.5, 0.75, 1.0, 1.25, 1.5, 1.75 and 2.0 % agarose gel at $E = 3.7 - 4.0$ V/cm in 0.1, 0.5 and 2.0× TBE for 90 – 120 min. (b) Ferguson plots of the AuNP size standards (samples in Lanes 1 – 4), in 0.5× TBE. Mobility M is in [$\text{cm}^2/\text{V}\cdot\text{s}$]. (c) Ferguson plots of the spheres (red squares), NRs (green circles), and short NRs (blue triangles) in 0.5× TBE. See Supporting Information for the plots with 0.1× and 2.0× TBE. (d) Plots of square root of the slope (K_R) from Ferguson plot vs. particle radius, obtained from the AuNPs of 4 different sizes in 0.1 (squares), 0.5 (circles) or 2.0× (triangles) TBE. This chart is used as the sizing standard for the rest of the samples.

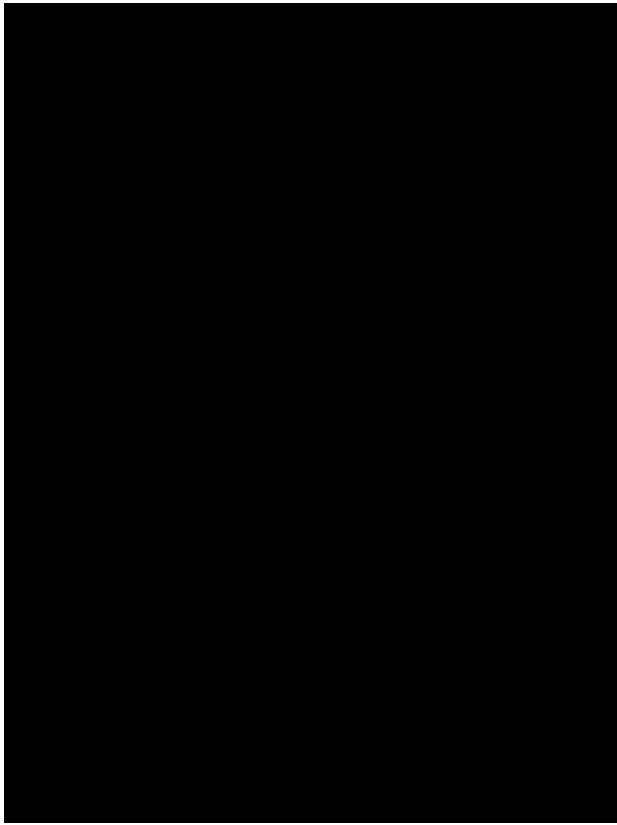


Figure 3. (a) Effective diameter (D_{eff}) of sphere, nanorod and short-nanorod in 0.1 (light gray), 0.5 (gray) and 2.0× TBE (dark gray) obtained by Ferguson analysis using the sizing standard in Figure 2c. Dimensions analyzed from TEM images are in black (diameter) and white (length) columns. (b) Free mobility M_0 of the samples in 0.1 (light gray), 0.5 (gray) and 2.0× TBE (dark gray) from the Ferguson plots. (c) ζ calculated from Henry's solution for spherical particle assumption; 0.1 (light gray), 0.5 (gray) and 2.0× TBE (dark gray). Ohshima's correction (cross hatched column) on spheres and Henry's solution for cylinders (white column) are placed next to the columns.

TABLES

Table 1. Concentration of reactants in [mM] and dimension (nm, \pm standard deviation) of gold nanorods from TEM images.

Sample	CTAB	NaCl	HAuCl ₄ ·3H ₂ O	AgNO ₃	AA	NaBH ₄	L × D, ave. aspect ratio
spheres	150	2.3	0.9	0	1.8	4×10 ⁻²	diameter: 24.1±3.9
NRs	150	2.3	0.9	0.18	1.8	2×10 ⁻³	(30.2±5.5)×(8.8±2.2), 3.52
short NRs	150	2.3	0.9	0.18	27	2×10 ⁻³	(27.5±4.8)×(15.4±3.7), 1.90

REFERENCES

- (1) Park, S.; Hamad-Schifferli, K. *ACS Nano* **2010**, *4*, 2555-2560.
- (2) Nel, A. E.; Mädler, L.; Velegol, D.; Xia, T.; Hoek, E. M. V.; Somasundaran, P.; Klaessig, F.; Castranova, V.; Thompson, M. *Nat. Mater.* **2009**, *8*, 543-557.
- (3) Ghosh, P.; Han, G.; De, M.; Kim, C.-K.; Rotello, V. M. *Adv. Drug Deliver. Rev.* **2008**, *60*, 1307-1315.
- (4) Alivisatos, P. *Nat. Biotechnol.* **2004**, *22*, 47-52.
- (5) Jain, P. K.; Lee, K. S.; El-Sayed, I. H.; El-Sayed, M. A. *J. Phys. Chem. B* **2006**, *110*, 7238-7248.
- (6) Huff, T. B.; Tong, L.; Zhao, Y.; Hansen, M. N.; Cheng, J.-X.; Wei, A. *Nanomed.* **2007**, *2*, 125-132.
- (7) Chen, C.-C.; Lin, Y.-P.; Wang, C.-W.; Tzeng, H.-C.; Wu, C.-H.; Chen, Y.-C.; Chen, C.-P.; Chen, L.-C.; Wu, Y.-C. *J. Am. Chem. Soc.* **2006**, *128*, 3709-3715.
- (8) Alper, J.; Crespo, M.; Hamad-Schifferli, K. *J. Phys. Chem. C* **2009**, *113*, 5967-5973.

- (9) Wijaya, A.; Schaffer, S. B.; Pallares, I. G.; Hamad-Schifferli, K. *ACS Nano* **2009**, *3*, 80-86.
- (10) Huang, X.; El-Sayed, I. H.; Qian, W.; El-Sayed, M. A. *J. Am. Chem. Soc.* **2006**, *128*, 2115-2120.
- (11) Gobin, A. M.; Lee, M. H.; Halas, N. J.; James, W. D.; Drezek, R. A.; West, J. L. *Nano Lett.* **2007**, *7*, 1929-1934.
- (12) Jana, N. R.; Gearheart, L.; Murphy, C. J. *Adv. Mater.* **2001**, *13*, 1389-1393.
- (13) Sau, T. K.; Murphy, C. J. *Langmuir* **2004**, *20*, 6414-6420.
- (14) Nehl, C. L.; Liao, H.; Hafner, J. H. *Nano Lett.* **2006**, *6*, 683-688.
- (15) Lu, Y.; Liu, G. L.; Kim, J.; Mejia, Y. X.; Lee, L. P. *Nano Lett.* **2005**, *5*, 119-124.
- (16) Wei, Q.; Song, H.-M.; Leonov, A. P.; Hale, J. A.; Oh, D.; Ong, Q. K.; Ritchie, K.; Wei, A. *J. Am. Chem. Soc.* **2009**, *131*, 9728-9734.
- (17) Zhang, Y.; Yang, M.; Portney, N. G.; Cui, D.; Budak, G.; Ozbay, E.; Ozkan, M.; Ozkan, C. S. *Biomed. Microdevices* **2008**, *10*, 321-328.
- (18) Win, K. Y.; Feng, S.-S. *Biomaterials* **2005**, *26*, 2713-2722.
- (19) Gratton, S. E. A.; Ropp, P. A.; Pohlhaus, P. D.; Luft, J. C.; Madden, V. J.; Napier, M. E.; DeSimone, J. M. *Proc. Natl. Acad. Sci. U.S.A.* **2008**, *105*, 11613-11618.
- (20) Verma, A.; Uzun, O.; Hu, Y.; Han, H.-S.; Watson, N.; Chen, S.; Irvine, D. J.; Stellacci, F. *Nat. Mater.* **2008**, *7*, 588-595.
- (21) Alkilany, A. M.; Nagaria, P. K.; Hexel, C. R.; Shaw, T. J.; Murphy, C. J.; Wyatt, M. D. *Small* **2009**, *5*, 701-708.
- (22) Lynch, I.; Cedervall, T.; Lundqvist, M.; Cabaleiro-Lago, C.; Linse, S.; Dawson, K. A. *Adv. Colloid Interface Sci.* **2007**, *134-135*, 167-174.

- (23) Ho, C. C.; Ottewill, R. H.; Yu, L. *Langmuir* **1997**, *13*, 1925-1930.
- (24) Dougherty, G. M.; Rose, K. A.; Tok, J. B.-H.; Pannu, S. S.; Chuang, F. Y. S.; Sha, M. Y.; Chakarova, G.; Penn, S. G. *Electrophoresis* **2008**, *29*, 1131-1139.
- (25) Park, S.; Hamad-Schifferli, K. *J. Phys. Chem. C* **2008**, *112*, 7611-7616.
- (26) Park, S.; Brown, K. A.; Hamad-Schifferli, K. *Nano Lett.* **2004**, *4*, 1925-1929.
- (27) Frens, G. *Nature Phys. Sci.* **1973**, *241*, 20-22.
- (28) Abramoff, M. D.; Magelhaes, P. J.; Ram, S. J. *Biophotonics Int.* **2004**, *11*, 36-42.
- (29) Wijaya, A.; Hamad-Schifferli, K. *Langmuir* **2008**, *24*, 9966-9969.
- (30) Rodbard, D.; Chrambach, A. *Proc. Natl. Acad. Sci. U.S.A.* **1970**, *65*, 970-977.
- (31) Aubin-Tam, M.-E.; Hwang, W.; Hamad-Schifferli, K. *Proc. Natl. Acad. Sci. U.S.A.* **2009**, *106*, 4095-4100.
- (32) Alper, J.; Hamad-Schifferli, K. *Langmuir* **2010**, *26*, 3786-3789.
- (33) Chakraborty, B.; Sha, R.; Seeman, N. C. *Proc. Natl. Acad. Sci. U.S.A.* **2008**, *105*, 17245-17249.
- (34) Henry, D. C. *Proc. R. Soc. Lond. A.* **1931**, *133*, 106-129.
- (35) Ohshima, H. *Theory of Colloid and Interfacial Electric Phenomena*, 1 ed.; Academic Press: London, 2006; Vol. 12.
- (36) De Keizer, A.; Van Der Drift, W. P. J. T.; Overbeek, J. T. G. *Biophys. Chem.* **1975**, *3*, 107-108.
- (37) Ohshima, H. *J. Colloid Interface Sci.* **1996**, *180*, 299-301.
- (38) Harris, L. B. *J. Colloid Interface Sci.* **1970**, *34*, 322-325.

- (39) Niidome, T.; Yamagata, M.; Okamoto, Y.; Akiyama, Y.; Takahashi, H.; Kawano, T.; Katayama, Y.; Niidome, Y. *J. Control. Rel.* **2006**, *114*, 343-347.
- (40) Rill, R. L.; Beheshti, A.; Winkle, D. H. V. *Electrophoresis* **2002**, *23*, 2710-2719.
- (41) Serwer, P. *Electrophoresis* **2005**, *10*, 327-331.

TABLE OF CONTENTS ONLY

